

DIFFERENTIAL ROTATION OF ϵ ERIDANI DETECTED BY *MOST*¹

Bryce Croll², Gordon A.H. Walker³, Rainer Kuschnig², Jaymie M. Matthews², Jason F. Rowe², Andrew Walker⁴, Slavek M. Rucinski⁵, Artie P. Hatzes⁶, William D. Cochran⁷, Russell M. Robb⁸, David B. Guenther⁹, Anthony F.J. Moffat¹⁰, Dimitar Sasselov¹¹, Werner W. Weiss¹²

ABSTRACT

The *Microvariability and Oscillations of STars (MOST)* photometric satellite observed three rotations of ϵ Eri continuously in late 2005. We detected two spots ($\Delta m \sim 0.01$) at different latitudes (20.0° , 31.5°) revolving with different periods (11.35, 11.55 d) from which we derive a differential rotation coefficient,

¹Based on data from the MOST satellite, a Canadian Space Agency mission, jointly operated by Dynacon Inc., the University of Toronto Institute of Aerospace Studies and the University of British Columbia with the assistance of the University of Vienna.

²Dept. Physics & Astronomy, UBC, 6224 Agricultural Road, Vancouver, BC V6T 1Z1, Canada; croll@interchange.ubc.ca, kuschnig@phas.ubc.ca, matthews@phas.ubc.ca, rowe@phas.ubc.ca

³1234 Hewlett Place, Victoria, BC V8S 4P7, Canada; gordonwa@uvic.ca

⁴Sumus Technology Ltd.; arwalker@sumusltd.com

⁵Dept. Astronomy & Astrophysics, David Dunlap Obs., Univ. Toronto P.O. Box 360, Richmond Hill, ON L4C 4Y6, Canada; rucinski@astro.utoronto.ca

⁶Thüringer Landessternwarte Tautenburg, Sternwarte 5, D-07778 Tautenburg, Germany; artie@tls-tautenburg.de

⁷McDonald Observatory, University of Texas at Austin, Austin, TX, 78712; wdc@astro.as.utexas.edu

⁸Physics & Astronomy, UVic, PO Box 3055, Victoria, BC V8W 3P6, Canada, robb@uvic.ca

⁹Department of Astronomy and Physics, St. Mary's University Halifax, NS B3H 3C3, Canada; guenther@ap.stmarys.ca

¹⁰Dépt de physique, Univ de Montréal C.P. 6128, Succ. Centre-Ville, Montréal, QC H3C 3J7, and Obs du mont Mégantic, Canada; moffat@astro.umontreal.ca

¹¹Harvard-Smithsonian Center for Astrophysics, 60 Garden Street, Cambridge, MA 02138, USA; sasselov@cfa.harvard.edu

¹²Institut für Astronomie, Universität Wien Türkenschanzstrasse 17, A-1180 Wien, Austria; weiss@astro.univie.ac.at

$k = 0.11_{-0.02}^{+0.03}$ in agreement with the prediction by Brown et al. (2004) for a young sun-like star having roughly twice the solar angular velocity. The light curve was analysed with the program StarSpotz, a modification of SPOTMODEL by Ribárik et al. (2003). The best fitting value for the inclination angle $i = 30^\circ \pm 3^\circ$ is compatible with inclinations already estimated for the disc ($\sim 25^\circ$) and planetary orbit (26.2°). The inclination also leads to an equatorial rotation speed of 3.42 km s^{-1} and the photometric value of $v \sin i = 1.7 \text{ km s}^{-1}$. When compared with spectroscopically determined values, the photometric $v \sin i$ allows, in principle, an independent estimate of the macroturbulent velocity. Both spots would have distorted the radial velocity curve $\sim \pm 10 \text{ m s}^{-1}$ by the Rossiter-McLaughlin effect which is similar to the stellar radial velocity 'noise' detected by others. Details are given of the StarSpotz model and of the uniqueness tests which we applied to arrive at a best solution and realistic estimates of errors in the derived parameters.

Subject headings: stars: activity — stars: individual (Epsilon Eri) — stars: late-type — stars: spots — stars: rotation — planetary systems

1. INTRODUCTION

ϵ Eridani ($V = 3.72$, HD 22049, HIP 16537, HR 1084), is the closest star (3.3 pc) to the Sun known to have a planetary companion (Hatzes et al. 2000). The planetary period is 6.9 years and Benedict et al. (2006) have estimated the planetary mass to be $1.5 M_{Jup}$ and an orbital inclination of 26.2° from *HST* astrometry and radial velocities. A 130 AU diameter dust ring surrounds the system inclined at $\sim 25^\circ$ (Greaves et al. (2000), Greaves et al. (2005)). An independent measurement of the stellar inclination axis from a quality light curve would provide important information on spin-orbit alignment in this system.

The star itself is K2 V and shows a high level of chromospheric activity (Gray and Baliunas 1995) consistent with a relatively young age of < 1 Gyr (Soderblom and Däppen 1989). Valenti et al. (1995) made a very careful infrared Zeeman analysis of the magnetic field and concluded that some 9% of the deep photosphere of ϵ Eri is covered by a 1.44 kG field. While there is some evidence that the field may vary (Saar 1988), Valenti et al. (1995) caution this may have more to do with differences in the adopted models and the relative sensitivities of optical and infrared measurements.

Several observers have found photometric variability of ϵ Eri attributable to its rotation. Vaughan et al. (1981) found a period of 11.8 d in the Ca II *K* line reversal and later,

Baliunas et al. (1983) found a period of 11.3 d. Frey et al. (1991), from a photometric campaign organised in the 1988/89 and 1989/90 observing seasons, found five single star spots each of which were visible for 1 to 2 months. The spots yielded rotation periods in the range $10.0 \text{ d} < P < 12.3 \text{ d}$ with amplitudes between 0.01 and 0.03 mag. From these they estimated a differential rotational coefficient very similar to the solar value.

The *MOST* photometric satellite (Walker et al. 2003) provides continuous photometry of target stars with unprecedented precision for weeks at a time. Rucinski et al. (2004) detected a pair of spots in the *MOST* light curve of κ^1 Ceti which had different rotation rates. In order to better decipher the spot activity and rotation of κ^1 Ceti based on the published 2003 *MOST* light curve, and two more obtained in 2004 and 2005, and to model spot distributions on other MOST targets, one of us, BC, has developed a program, Starspotz which is described below. The program is also expected to help in the search for spots in other stars and help define their evolution.

It has long been recognised that differential rotation and convection provide the engine for the solar dynamo (see for example Ossendrijver (2003)). Schau et al. (1998) found from analysis of Doppler images taken with the *Solar and Heliospheric Observatory (SOHO)* that the decrease of angular velocity with latitude seen at the solar surface extends with little radial variation through much of the convective layer with a transition to nearly uniform rotation in the radiative interior through an adjustment layer called the tachocline. Angular momentum is continually redistributed in the convective envelope, which covers about one third of the solar radius, resulting in the marked differential rotation seen at the surface (Brun and Toomre 2002).

It is assumed that, when younger, the sun rotated more rapidly and gradually lost angular momentum through magnetic coupling to the solar wind. Calculations by Brown et al. (2004) indicate that there should be a systematic decrease of angular velocity contrast with increasing angular velocity for solar-type stars. The simultaneous detection of two or more spots at different latitudes in *MOST* light curves of solar-type stars having sufficiently short rotation periods allows us to directly measure differential rotation for stars with different ages and angular velocities - a valuable adjunct to understanding the interior rotation of the sun and solar-type stars.

In this paper we introduce, and give details of, the program StarSpotz and derive an inclination of the rotation axis to the line of sight, equatorial speed, $v \sin i$ and differential rotation rate for ϵ Eri.

2. THE *MOST* PHOTOMETRY

The *MOST* satellite was launched on June 2003 and is fully described by Walker et al. (2003). A 15/17.3 cm Rumak-Maksutov telescope feeds two CCDs, one for tracking and the other for science, through a single, custom, broadband filter (350 – 700 nm). Starlight from Primary Science Targets ($V \leq 6$) is projected onto the science CCD as a fixed (Fabry) image of the telescope pupil covering about 1500 pixels for high photometric stability and insensitivity to detector flatfield irregularities and the effect of particle irradiation on individual pixels. The experiment was designed to detect photometric variations with periods of minutes at micro-magnitude precision and does not rely on comparison stars or flat-fielding for the Fabry photometry. There is no direct connection to any photometric system. Tracking jitter was dramatically reduced by early 2004 to ~ 1 arcsec which led to significantly higher precision in the Fabry photometry.

The observations received from the satellite were reduced by RK. Outlying data points generated by poor tracking or cosmic ray hits were removed. *MOST* suffers from parasitic light, mostly Earthshine, at certain orbital phases, with the amount and phase depending on the stellar coordinates, spacecraft roll and season of the year. Data are also recorded for Fabry images from seven of the eight lenses adjacent to the target Fabry lens in order to track the stray light background. These background signals were combined in a mean and subtracted from the target photometry. This also corrected for bias, dark and background signals and their variations. The reductions basically followed the scheme already outlined by Rucinski et al. (2004)

MOST observed ϵ Eri from from 2005 Oct 28 till Dec 3 - a total of 35.7 days. More than 120,000 data points were collected with exposure times of 20 seconds sampled every 25 seconds. Even with data points subject to high background/straylight and other outliers (SAA, bad pointing) removed, the overall duty cycle was 88% with the longest gap being 3.5 hours. The intrinsic point-to-point precision in the unbinned light curve was 250 ppm rms.

For the star spot analysis, the data were binned at the *MOST* orbital period of 101.413 min. Figure 1 displays the full light curve with time in JD (heliocentric). Here, the point-to-point precision is 50 ppm rms. The solid line in the lower panel displays the mean background per orbit as a function of date while the two most divergent background readings from the seven background Fabry images are shown as thin dotted and dashed lines. There is no obvious correlation between structure in the parasitic background signal and the light curve. The complete light curve can be downloaded from the *MOST* Public Archive at www.astro.ubc.ca/MOST/.

A much more detailed analysis of the unbinned data of ϵ Eri has been carried out by

Guenther et al. (2006) in a search for sun-like p-mode oscillations with periods of minutes. In this case, parasitic light effects were aggressively removed at all satellite orbital phases according to the scheme of Reegen et al. (2006). Full details are given in Guenther et al. (2006).

3. StarSpotz

One of us, BC, has developed the program, StarSpotz, to return the most physically plausible configuration of starspots from an analytical fitting of models to a given light-curve. The StarSpotz program is based on the SPOTMODEL program of Ribárik et al. (2003), and is intended as a modification and improvement designed specifically to handle the nearly continuous photometry returned by *MOST*. StarSpotz includes much of the key functionality of the SPOTMODEL program, as well as improvements and other features necessary to fit the characteristics of the *MOST* light curves.

StarSpotz, like SPOTMODEL, uses a Marquardt-Levenberg non-linear least squares algorithm to fit the observed light-curves to the analytic models of Budding (1977) or Dorren (1987). Both these models return the theoretical light-intensity as a function of time, $l_c(t)$, due to the effect of one or more non-overlapping uniform circular spots. Extending the model to include spots with umbra/penumbra as described by Budding (1977) or Dorren (1987) has not been attempted in this first application. The two relevant stellar input parameters are given in Table 1, while the input parameters for each individual spot are listed in Table 2.

Table 1. StarSpotz: stellar input parameters

| var | definition |
|-----|--|
| i | inclination of rotation axis to line of sight ($^{\circ}$) |
| U | unspotted intensity of the star |

Table 2. StarSpotz: spot input parameters

| var | definition |
|------------|---|
| λ | spot longitude (0° to 360°) |
| β | spot latitude (-90° to 90°) |
| γ | spot angular radius (0° to 90°) |
| p | spot period in days |
| E | spot epoch HJD |
| κ_w | flux ratio between spot and unspotted photosphere (0-1) |
| u | linear limb darkening coefficient (0-1) |

The main fitting method adapted from the SPOTMODEL program is the standard Spot Model (§3.3).

3.1. Documentation and Release information

The StarSpotz program was developed in the Visual C++ environment for the Windows platform. The main StarSpotz window gives a view of the data, model, and spot configuration as it changes with the fitting process. OpenGL is used to draw the star and the spot configuration from the various viewpoints.

The StarSpotz program includes other useful functionality to return the most relevant configuration of starspots for observed photometry. The full source-code, executable, and documentation for the first and subsequent releases of this program are available at www.astro.ubc.ca/MOST/StarSpotz/.

3.2. Budding and Dorren Models

Budding (1977) estimated the drop in light intensity caused by a circular spot. He defined σ integrals for the area projected on the line of sight. The integrals are:

$$\sigma_n^m = \frac{1}{\pi} \int \int_{spot\ area} x^m z^n dx dy \quad (1)$$

σ_0^0 ($m = 0, n = 0$) represents the projected area of the spot, while σ_1^0 ($m = 0, n = 1$) represents the effect of linear limb darkening. The xyz cartesian coordinate system orients the z-axis towards the observer. This cartesian coordinate system can be related to the spherical polar system of longitude, λ , and latitude, β .

Budding (1977) further defined the spot-darkening function, related to the linear limb darkening coefficient u by:

$$\sigma_c = \frac{3}{3-u} [(1-u)\sigma_0^0 + u\sigma_1^0] \quad (2)$$

The intensity of the spotted star is thus related to the unspotted intensity of the star, U , by:

$$I_c(t) = U \left[1 - \sum_{j=1}^{N_{SPOTS}} (1 - \kappa_{\omega_j}) \sigma_c(u_j, \lambda_j, \beta_j, \gamma_j) \right] \quad (3)$$

where the j subscript represents the characteristics of the j^{th} spot. Where differential rotation is observed, longitude is an ambiguous concept and the spot location is defined better by the period, p , and epoch, E , while setting $\lambda = 0$.

The model defined by Dorren (1987) is similar to the model defined by Budding (1977). The differences between the two in terms of accuracy and computational efficiency are negligible, and thus it is left as a matter of preference for the user which model to select. Budding's model will be used in this paper.

3.3. Standard Spot Model

The standard spot model attempts to use the analytic spot models of Budding (1977) or Dorren (1987) to fit the observed light-curve. The apparent magnitude of the star, $l_o(t)$ is fitted to the theoretical magnitude, $l_c(t)$, as returned by one of the two models. The optimal configuration of starspots is obtained by minimizing the sum of squared residuals:

$$\chi^2 = \sum_{i=1}^N \frac{(l_{o_i} - l_{c_i})^2}{(\Delta l_{o_i})^2} \quad (4)$$

The fitting process ends when the difference in the sum of squared residuals falls below a user-specified amount. The fitted parameters are returned with errors as determined by the square-root of the diagonal elements of the covariance matrix when the reduced χ^2 is approximately 1.0. In the case the fitted parameters are correlated, as is often the case in photometric spot modeling, the off-diagonal elements of the covariance matrix are often non-zero and the returned uncertainties will be underestimates.

3.4. Uniqueness Tool

The non-uniqueness of photometric spot modeling is a well-known limitation of the photometric method. The uniqueness tool is an attempt to define the uniqueness of a given photometric spot-model solution by implementing a simple technique to search for other local minima in χ^2 space. Specifically the tool searches for other solutions that may fit the light curve as well or better than the given solution. In the case that the fitted parameters are correlated, the uncertainty tool returns more realistic uncertainties in the spot parameters via Monte Carlo statistics than does the Standard Spot Model (§3.3).

The uniqueness tool uses the user-defined best-fit model (henceforth the initial model) as its starting point while it attempts to search for other solutions that fit the light-curve as

well as, or better than, the initial model. The initial conditions for the Standard Spot Model are set as a modest variation from the initial model, with the spots randomly dispersed around the star.

For instance, a one-spot solution with set U , i , κ_w and u , can be investigated, by setting the initial conditions for the new period, longitude, latitude and size of the spot as: $p_{new} = p_o \pm \delta p$, $\lambda_{new} = \delta \lambda$, $\beta_{new} = \delta \beta$, and $\gamma_{new} = \delta \gamma$, where δp , $\delta \lambda$, $\delta \beta$, and $\delta \gamma$ are user-defined, appropriately-sized random variables. The Standard Spot Model fitting process is then implemented. If the parameters returned by the fit result in a sum of squared residuals that is suitably close to, or lower than, the initial model, the returned parameters are recorded.

This process is repeated as many times as necessary to generate adequate statistics. Through this process the uniqueness of the best-fitting solution can be estimated. Solutions may be returned that fit the data as well or better than the initial model. These alternate spot configurations can be investigated for physical plausibility.

By generating sufficient statistics, the uniqueness tool also gives better estimates of the true uncertainties in the fitted parameters. This is helpful because the effect of changing one parameter in photometric spot-modeling is often closely correlated to the effect of changing an alternate parameter; as a result the errors returned by the Standard Spot Model (§3.3) are often underestimates. By generating numerous examples of the same relative configuration of starspots, Monte Carlo statistics can be generated that return more realistic uncertainties.

4. THE SPOTS ON ϵ ERI

Before analysing the *MOST* ϵ Eri light curve shown in Figure 1, a small linear trend of $8.1328 \times 10^{-5} \text{ d}^{-1}$ was removed. The latter was established by normalising the first and third maxima to 1. Since we are only interested in star spots which are expected to have rotation periods between 10 and 12 days, longer period trends, whether instrumental or intrinsic to the star can be ignored.

Using the interactive display it soon became clear that a two spot model, with an inclination of $\approx 30^\circ$ provided the best fit; the StarSpotz Standard Model was thus applied by adopting two circular spots. The adopted linear limb-darkening coefficient, $u = 0.811$, and flux ratio between the spot and unspotted photosphere $\kappa_w = 0.220$ were based on compilations of Díaz-Cordovés et al. (1995). The results of the Standard Model analysis are given in Table 3. The fitted spot configuration and residuals from the fit to the light curve are shown in Figure 2. Figure 3 shows the amplitude spectra of the light curve before (dots),

and after (dashes), removing the model. The residuals obviously contain no periodicity in the expected range of rotational period and so the solution was not extended to more than two spots. We have not attempted to improve the fit using non-circular spots, or by including umbra/penumbra.

4.1. ϵ Eri Uniqueness test

The uniqueness test (§3.4) was applied to the ϵ Eri data to search for other two-spot solutions that fit the observed light curve as well as, or better than, the Table 3 model. The solution in Table 3 was used as the initial solution. The parameters that were fitted and the range added to the Table 3 parameters for the initial condition of the fit are given in Table 4. All other parameters are the same as in Table 3. The range in the fitted parameters as given in Table 4 were chosen by trial and error. They are believed to be sufficiently large to allow for all physically plausible solutions to be returned. The standard spot model was allowed to continue for 3000 iterations, or until the change in reduced χ^2 per degree of freedom fell below 10^{-21} . The returned solution was recorded if the reduced χ^2 was within $\approx 4\%$ of the Table 3 solution (reduced $\chi^2 < 295$). This value was chosen by visual inspection, as solutions with reduced χ^2 below this value appeared to give reasonable fits to the light curve. The inclination angle was assumed to be between 25° and 35° . An additional constraint was added that the unspotted intensity of the star, U , had to be at least 1.000 - the maximum signal observed.

The uniqueness results representing all other two-spot solutions to the observed light curve are given in Table 5. We adopt solution 1 as the most appropriate. Solution 1 is identical (within the uncertainty) to our presented solution as given in Table 3, and presented in Figure 2. Solution 2 requires a giant spot over the visible pole, where light modulation is generated by only a slight asymmetry in the spot's location toward the observer at the epoch of minimum signal. Solutions 3 and 4 each require a huge spot covering most of the largely non-visible hemisphere and one smaller spot in the upper hemisphere. Modulation of the light curve is generated primarily by the visible rim of the larger spot. These other solutions, although mathematically valid seem physically implausible.

Table 3. Spot parameters for ϵ Eri from the Standard Model analysis

| Parameter | Fitted | Value ^a |
|--|--------|--------------------|
| reduced χ^2 | n/a | 282.80 |
| ν^b | n/a | 485 |
| i | no | 30.0 |
| U | no | 1.0000 |
| $\kappa_{\omega 1}, \kappa_{\omega 2}$ | no | 0.220 |
| u_1, u_2 | no | 0.811 |
| E_1 | yes | 2130.34 ± 0.13 |
| p_1 | yes | 11.35 ± 0.03 |
| β_1 | yes | 20.0 ± 3.2 |
| γ_1 | yes | 6.2 ± 0.13 |
| E_2 | yes | 2126.42 ± 0.11 |
| p_2 | yes | 11.55 ± 0.02 |
| β_2 | yes | 31.5 ± 2.1 |
| γ_2 | yes | 7.2 ± 0.07 |

^a1- σ errors are those returned by the standard spot model (§3.3), where reduced χ^2 has been scaled to one; as the off-diagonal elements of the covariance matrix are non-zero these errors are likely underestimates.

^b ν is the number of binned data points minus the number of fitted parameters (eight in this case).

Table 4. Summary of Uniqueness test initial conditions for ϵ Eri

| Parameter | Initial Value ^a | Fitted | Range or constant value of δ_j |
|----------------------|----------------------------|--------|---------------------------------------|
| i | $i_o + \delta_i$ | no | $[-5.0^\circ, 5.0^\circ]$ |
| <i>offset</i> | $U_o + \delta_U$ | yes | $[-0.0015, 0.0015]$ |
| p_1, p_2 | $p_{io} + \delta_p$ | yes | $[-1.0, 1.0 \text{ d}]$ |
| E_1, E_2 | $E_{io} + \delta_E$ | yes | $[-1.0, 1.0 \text{ d}]$ |
| β_1, β_2 | δ_β | yes | $[0^\circ, 70^\circ]$ |
| γ_1, γ_2 | δ_γ | yes | 0.1° |

^aThe subscript ($_o$) refers to the associated parameter in Table 3.

Table 5. Two spot uniqueness solutions for ϵ Eri from Starspotz analysis

| # ^a | reduced χ^2 ^b | inclination i | offset U | epoch E | period p | latitude β | size γ |
|----------------|----------------------------------|--------------------|---------------------|---------------------|---------------------|---------------------|------------------|
| 01 | 282.796 | 30.0 ± 2.9 | 1.0000 ± 0.0001 | 2130.336 ± 0.01 | 11.350 ± 0.0013 | 20.0 ± 2.4 | 6.3 ± 0.4 |
| | | | | 2126.414 ± 0.01 | 11.554 ± 0.0005 | 31.4 ± 3.4 | 7.3 ± 0.4 |
| 02 | 265.800 | 29.8 ± 2.9 | 1.4994 ± 0.0660 | 2127.451 ± 0.00 | 11.555 ± 0.0017 | 89.0 ± 0.3 | 55.5 ± 5.2 |
| | | | | 2143.111 ± 0.01 | 19.269 ± 0.0147 | -30.8 ± 1.6 | 20.4 ± 1.9 |
| 03 | 281.222 | 31.4 ± 3.0 | 1.0002 ± 0.0001 | 2130.412 ± 0.02 | 11.343 ± 0.0018 | 20.8 ± 2.5 | 6.0 ± 0.5 |
| | | | | 2126.454 ± 0.01 | 11.552 ± 0.0011 | -80.6 ± 0.3 | 73.6 ± 2.3 |
| 04 | 285.647 | 32.1 ± 1.0 | 1.0003 ± 0.0004 | 2130.360 ± 0.09 | 11.352 ± 0.0070 | -79.6 ± 0.1 | 68.0 ± 0.9 |
| | | | | 2126.417 ± 0.04 | 11.553 ± 0.0034 | 35.3 ± 4.0 | 7.0 ± 0.1 |

^aOver 16,500 individual solutions with reduced $\chi^2 < 295$ were returned, all of which could be classified as one of these spot configurations. 1- σ errors are given.

^b ν was set to be 485 for comparison with the χ^2 values in Table 3. ν properly should be 484 for the uniqueness test as there was an additional free parameter (the unspotted intensity of the star U).

5. DISCUSSION

We consider the two spot solution 1 from Table 5 to be the best and, as a result of the uniqueness test, we have credible errors in the various spot and stellar parameters.

5.1. Differential Rotation

Frey et al. (1991) extracted the differential rotation coefficient, k , from the standard expression:

$$P_\phi = P_{\text{EQ}}/(1 - k \sin^2\phi) \quad (5)$$

where P_ϕ and P_{EQ} are the rotation periods at latitude ϕ and on the stellar equator, respectively. In their study of ϵ Eri they determined rotation periods between 10 and 12.3 d for twelve individual spots seen over two years by fitting sine curves to twelve different segments of the light curve. By assuming that the spots covered the full range of ϕ between 0° and 90° and that the period range was the result of differential rotation, they derived $k = 0.2 \pm 0.05$ - a result closely similar to solar (0.19).

Using the StarSpotz program on the *MOST* light curve we have detected two spots simultaneously as well as a value of i . The solution provides both latitudes and rotation periods from which we derive a value of $k = 0.11_{-0.02}^{+0.03}$ with no ambiguity in the sign of k . The limits are set by the $1\text{-}\sigma$ range in the value of k for solution 1 of the uniqueness tests. This value of k is fairly robust and, being only half solar, it agrees remarkably well with the prediction by Brown et al. (2004) (their Figure 2) for a younger sun having twice the angular velocity. In fact, from the numbers in the next section the angular velocity of ϵ Eri is about a factor of 2.25 greater than solar. There is clearly a strong case to follow up these observations in another season and for other solar-type stars.

5.2. $v \sin i$ and equatorial speed

Fischer and Valenti (2005) list values of $R_{\epsilon\text{Eri}} = 0.76R_\odot$ and $v \sin i = 2.45 \text{ km s}^{-1}$ for ϵ Eri. Taking $k = 0.11$ gives $P_{\text{EQ}} = 11.20 \text{ d}$ and an equatorial speed of 3.42 km s^{-1} and for $i = 30^\circ$, $v \sin i = 1.7 \text{ km s}^{-1}$. Valenti et al. (1995) in their modeling for the infrared Zeeman pattern took a value of $v \sin i = 1 \text{ km s}^{-1}$ (coincident with that of Marcy and Basri (1989)) and a microturbulence of 1.25 km s^{-1} . It should be noted that our value of $v \sin i$ is based entirely on photometry and the estimate of R_\odot making it insensitive to the magnitude of either the micro-, or macro-turbulent velocities. Fischer and Valenti (2005) quote a median

error of $\sim 3\%$ in R_{\odot} .

Archival spectroscopic observations from the McDonald Observatory of ϵ Eri taken at $R=220,000$ are of higher resolution than those available to Fischer and Valenti (2005). Line profiles in ϵ Eri are narrower than in the sun. We have tried a simple $v \sin i$ fit to the Fe I $\lambda 6256$ line. Because of the low $v \sin i$, there is a trade off between macroturbulence and rotational velocity as mentioned in the preceding paragraph. According to Gray (1992) a G2 V star would have a macroturbulent velocity of $\sim 4 \text{ km s}^{-1}$ and a K2 V about $\sim 2 \text{ km s}^{-1}$. For a microturbulent velocity of 3 km s^{-1} the McDonald Observatory line profile implies $v \sin i = 2.5 \text{ km s}^{-1}$ and 3 km s^{-1} for a microturbulent velocity of 2.5 km s^{-1} . Given the uncertainties in the value of the microturbulent velocity, the photometric value of $v \sin i = 1.7 \text{ km s}^{-1}$ is consistent with the spectroscopic value. A full $v \sin i$ analysis requires the right model atmosphere, and appropriate Fourier analysis but, in principle, we should be able to derive an independent value for the macroturbulent velocity using the photometrically determined value of $v \sin i$.

5.3. Rotation axis inclination and possible Rossiter-McLaughlin effect

Our value for the inclination, $i = 30^\circ$, of the stellar rotation axis to the line of sight is close to those determined for the planetary and disc axes but lacks an independent measurement of the azimuthal projection angle so we cannot say whether our value of i supports a measure of spin-orbit coupling.

There was no simultaneous spectroscopic campaign accompanying the *MOST* observations but it is interesting to note two things. First, the fractional surface area covered by the two spots is similar to the fractional surface coverage of the 1.44 kG field (Valenti et al. 1995). One cannot draw many conclusions from this except that the active areas were of similar size at these different epochs.

The second implication of the two spots is that during transit they would have introduced distortions of the radial velocity curve by the Rossiter-McLaughlin effect (Rossiter 1924). The individual S-shaped distortion signals would have been on the order of half the revolution time of each spot, 5.5 d. Winn et al. (2005) very elegantly measured the characteristic S-shaped distortion of the radial velocity curve by the transit of the exo-planet in HD 209458. The effect arises from the imbalance in the contributions of stellar rotation to the stellar line profiles from each limb. In the case of HD 209458, the eclipse depth is $\sim 1\%$ and $v \sin i = 4.7 \text{ km s}^{-1}$. Winn et al. (2005) detected excursions $\sim \pm 40 \text{ m s}^{-1}$.

In the case of the spots on ϵ Eri, the individual spot intensities are $\sim 1\%$ and $v \sin i =$

1.7 km s⁻¹ which, by analogy with the work of Winn et al. (2005), could lead to distortions $\sim \pm 10$ m s⁻¹. The distortion signal would be complicated by the presence of the two spots and essentially appear as noise in the radial velocity curve. Such a level of noise plagued early attempts to detect a planetary companion to ϵ Eri (Hatzes et al. 2000).

Our analysis of the ϵ Eri *MOST* light curve indicates that StarSpotz is a powerful tool when coupled with high quality photometry allowing one to determine differential rotation (when two or more spots are detected), axial inclination, equatorial rotational speed and $v \sin i$.

The Natural Sciences and Engineering Research Council of Canada supports the research of B.C., D.B.G., J.M.M., A.F.J.M., J.F.R., S.M.R., G.A.H.W.. Additional support for A.F.J.M. comes from FCAR (Québec). R.K. and A.W. are supported by the Canadian Space Agency. W.W.W. is supported by the Austrian Space Agency and the Austrian Science Fund (P14984).

REFERENCES

- Baliunas, S.L., Hartmann, L., Noyes, R.W., Vaughan, H., Preston, G.W., Frazer, J., Lanning, H., Middelkoop, F., Mihalas, S. 1983, ApJ, 275, 752
- Benedict, G. F., McArthur, B.E., Gatewood, G., Nelan, E., Cochran, W.D., Hatzes, A., Endl, M., Wittenmyer R., Baliunas S.L., Walker, G.A.H, Yang, S., Kürster, K., Els, S., Paulson, D.B. 2006, ApJ, submitted.
- Brown, B. P., Browning, M. K., Brun, A. S., Toomre, J. 2004, Proceedings of the SOHO 14 / GONG 2004 Workshop (ESA SP-559). "Helio- and Asteroseismology: Towards a Golden Future". 12-16 July, 2004. New Haven, Connecticut, USA. Editor: D. Danesy., p.341
- Brun A.S., Toomre J. 2002, ApJ, 570, 865
- Budding, E. 1977, Ap&SS, 48, 207
- Díaz-Cordovés, J., Claret, A., Giminénez, A. 1995, Ap&SS, 110, 329
- Dorren, J.D. 1987, ApJ, 320, 756
- Fischer, D.A., Valenti, J. 2005, ApJ, 622, 1102

- Frey, G.J., Hall, D.S., Mattingly, P., Robb, S., Wood, J., Zeigler, K., Grim, B. 1991, *AJ*, 102, 1813
- Gray, D.F. 1992, *The Observations and Analysis of Stellar Photospheres* (Cambridge: Cambridge Univ. Press)
- Gray, D. F., & Baliunas, S. L. 1995, *ApJ*, 441, 436
- Greaves, J. S., et al. 2005, *ApJ*, 619, 187
- Greaves, J. S., et al. 1998, *ApJ*, 506, 133
- Guenther, D. B., Kallinger, T., Reegen, P., Weiss, W. W., Matthews, J.M., Kusching, R., Moffat, A.F.J., Rucinski, S.M., Sasselov, D., Walker, G.A.H. 2006, *ApJ*, submitted
- Hatzes, A.P., Cochran, W.D., McArthur, B., Baliunas, S.L., Walker, G.A.H., Campbell, B., Irwin, A.W., Yang, S., Kürster, M., Endl, E., Els, S., Butler, R.P., Marcy, G.W. 2000, *ApJ*, 544, 145
- Marcy, G.W., Basri, G. 1989, *ApJ*, 345, 480
- Matthews, J.M., Kusching, R., Guenther, D.B., Walker, G.A.H., Moffat, A.F.J., Rucinski, S.M., Sasselov, D., Weiss, W.W. 2004, *Nature*, 430, 51
- Ossendrijver, M. 2003, *Astronomy and Astrophysics Review*, Volume 11, Issue 4, 287
- Reegen, P., Kallinger, T., Frast, D., Gruberbauer, M., Huber, D., Matthews, J. M., Punz, D., Schraml, S., Weiss, W. W., Kuschnig, R., Moffat, A. F. J., Walker, G. A. H., Guenther, D. B., Rucinski, S. M., Sasselov, D. 2006 *MNRAS*, in press
- Ribárik, G., Oláh, K., Strassmeier, K. G. 2003, *Astronomische Nachrichten*, 324, 202
- Rossiter, R.A. 1924, *ApJ*, 60, 15
- Rucinski, S.M., Walker, G. A. H., Matthews, J.M., Kuschnig, R., Shkolnik, E., Marchenko, S., Bohlender, D.A., Guenther, D. B., Moffat, A. F. J., Sasselov, D., Weiss, W. W. 2004, *PASP*, 116, 1093
- Saar, S.H. 1988, 324, 441
- Schau, J., et al. 1998, *ApJ*, 505, 390
- Soderblom, D. R., & Däppen, W. 1989, *ApJ*, 342, 945
- Strassmeier, K.G., Bartus, J. 2000, *A&A*, 354, 537

- Valenti, J.A., Marcy, G.F., Basri, G. 1995, *ApJ*, 439, 939
- Vaughan, A.H., Preston, G.W., Baliunas, S.L., Hartmann, L.W., Noyes, R.W., Middelkoop, F., Mihalas, D. 1981, *ApJ*, 250, 276
- Walker, G. A. H., Matthews, J., Kuschnig, R., Johnson, R., Rucinski, S., Pazder, J., Burley, G., Walker, A., Skaret, K., Zee, R., Grocott, S., Carroll, K., Sinclair, P., Sturgeon, D., Harron, J. 2003, *PASP*, 115, 1023
- Winn, J.N., Noyes, R. W., Holman, M.J., Charbonneau, D., Ohta, Y., Taruya, A., Suto, Y., Narita, N., Turner, E.L., Johnson, J. A., Marcy, G. W., Butler, R. P., Vogt, S.S. 2005, *ApJ*, 631, 1215

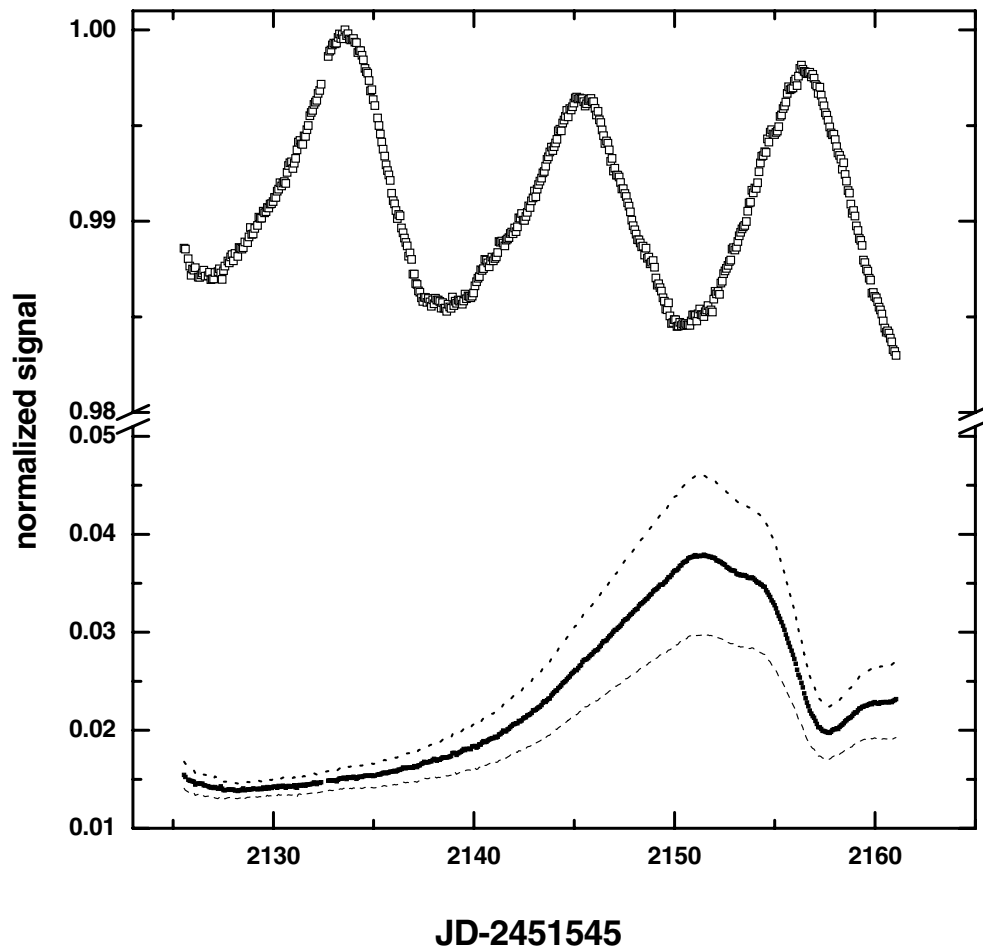


Fig. 1.— The ϵ Eri light curve observed by *MOST* in 2005. The data have been binned at the *MOST* orbital period of 101.413 min. Dates are Heliocentric JD. The point to point precision is 50 ppm rms. The solid line in the lower panel displays the evolution of the mean background per orbit subtracted from the original data and derived from seven background Fabry images. The two most divergent background readings are shown by dotted and dashed lines.

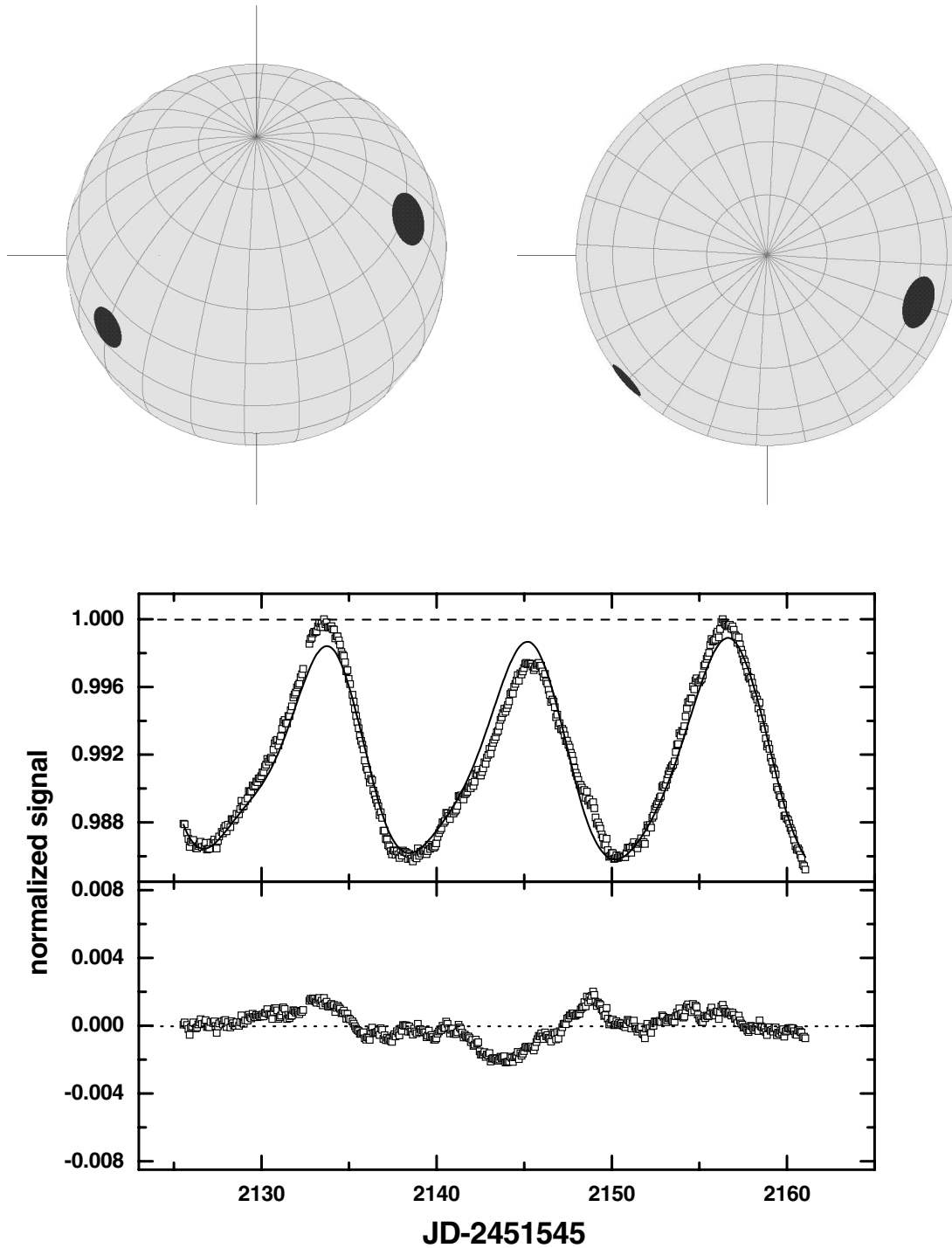


Fig. 2.— Top: ϵ Eri spots (Table 3) as seen from the line of sight (left), and the visible pole (right). Middle: the light curve of Figure 1 with a linear trend removed. The solid line is the model from Table 3. The dashed line indicates the unspotted intensity of the star ($U=1.0000$). Bottom: residuals from the model on the same scale.

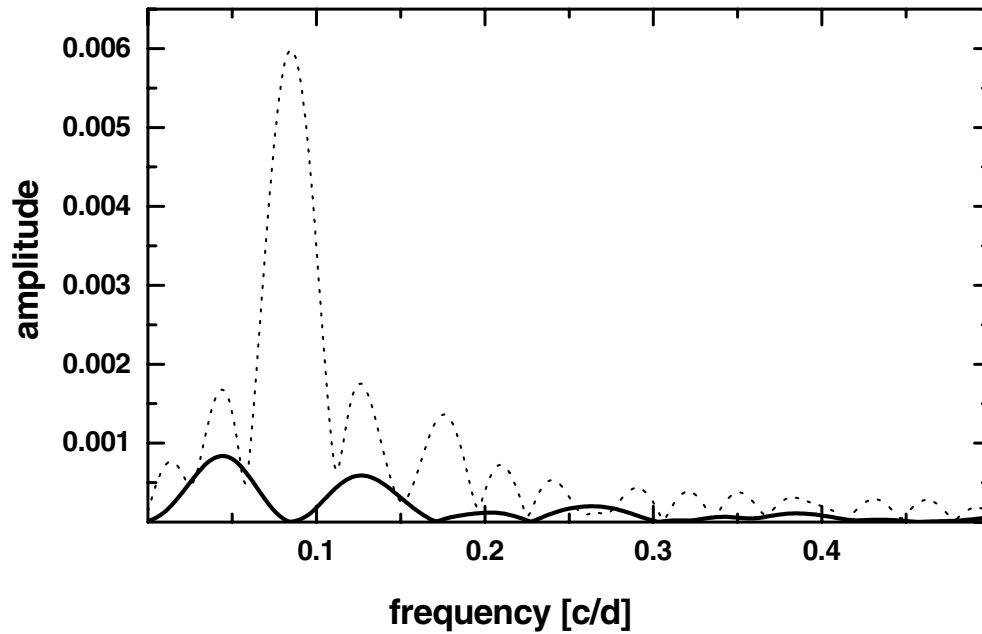


Fig. 3.— Amplitude spectra of the model (dashed) of Figure 2 and of the residuals from the model (solid), demonstrating that no signal remains in the residuals over the range of rotational rates (0.088 ± 0.012 cycles/day) expected for ϵ Eri.